Supplementary Information for:

Macrophages Reprogramming Combined with Enhanced Photodynamic Therapy Increase Patency of Malignant Esophageal Obstruction after Stenting

Haoyang Xu, ‡[a] Yiran Zhang, ‡[a] Sheng Guo,[a] Hui Fang, [a] Liming Wei,[a] Guangchen He,[a] Yingsheng Cheng[b] and Yueqi Zhu *[a]*

[a] The Department of Radiology;Shanghai Sixth People's Hospital Affiliated to Shanghai Jiao Tong University School of Medicine;No. 600, Yishan Road; Shanghai, 200233, P. R. China.

[b] The Department of Imaging Medicine and Nuclear Medicine;Tongji Hospital of Tongji University;No.389, Xincun Road; Shanghai, 200065, P. R. China

*** Corresponding author**. Contact: E-mail: zhuyueqi@sjtu.edu.cn;Tel.: +86-21-66301136; Fax: +86-21-66303983

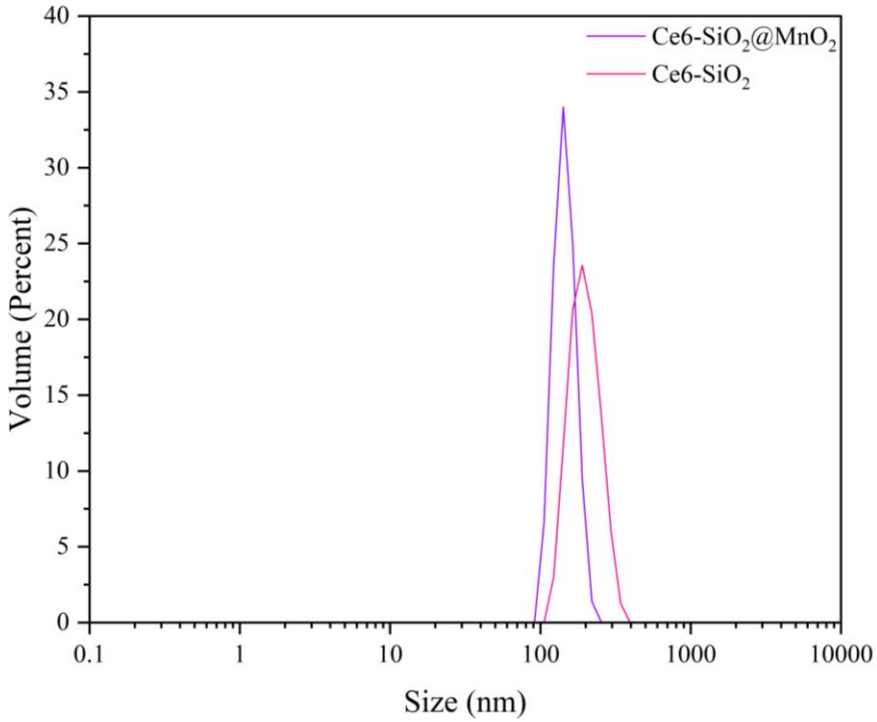

Figure S1. Particle size distribution of Ce6-SiO_2@MnO_2 and SiO_2-Ce6**.**

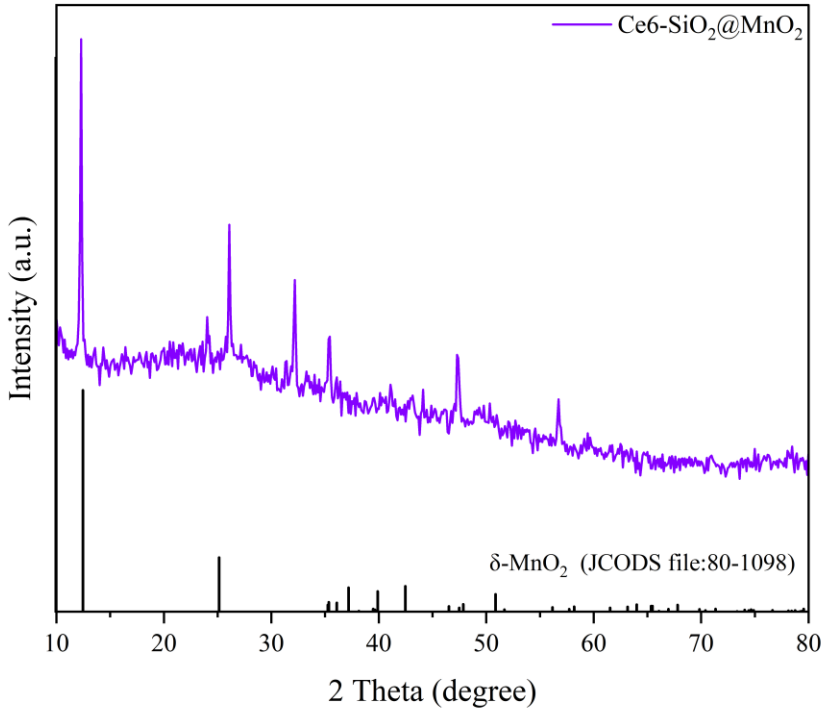

Figure S2. X-ray diffractometer patterns of Ce6-SiO_2@MnO_2 and δ-MnO2.

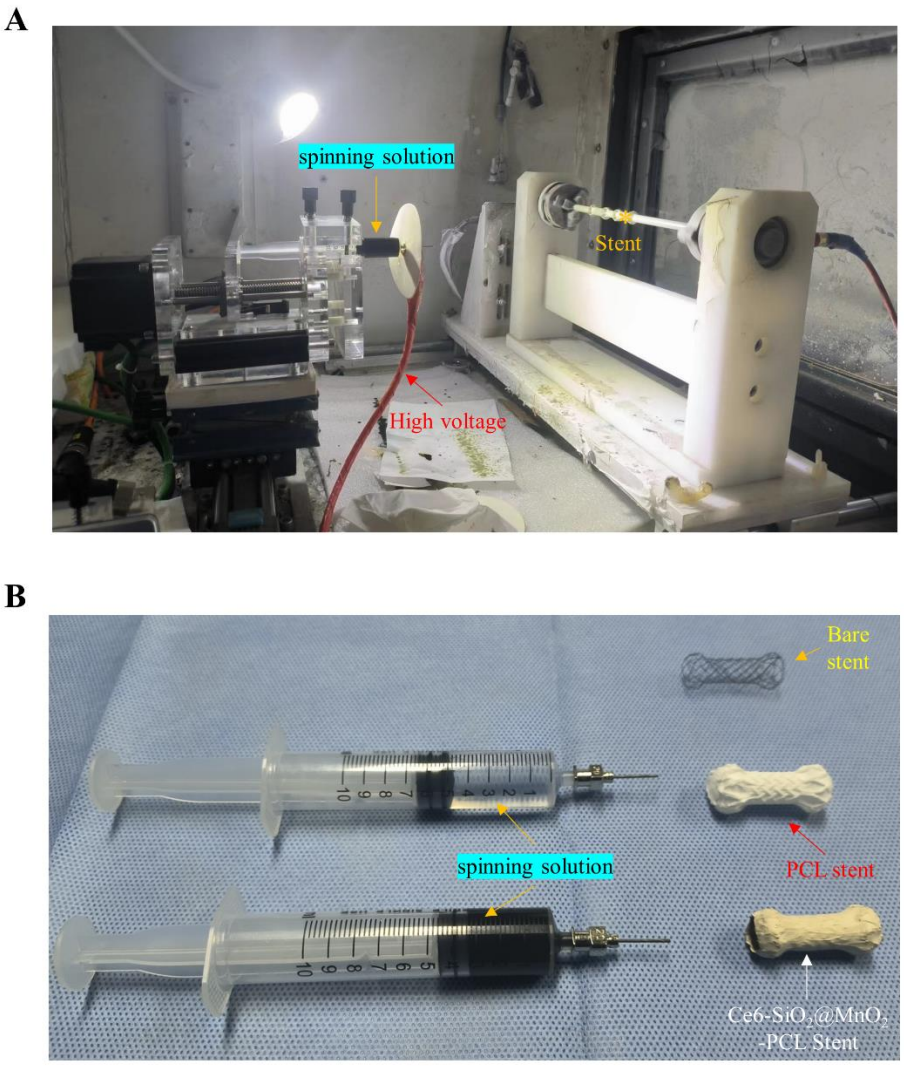

Figure S3. The process of electrospinning. A) Representative photo of the electrospinning process. B) Photo of the spinning solution with corresponding coated stent.

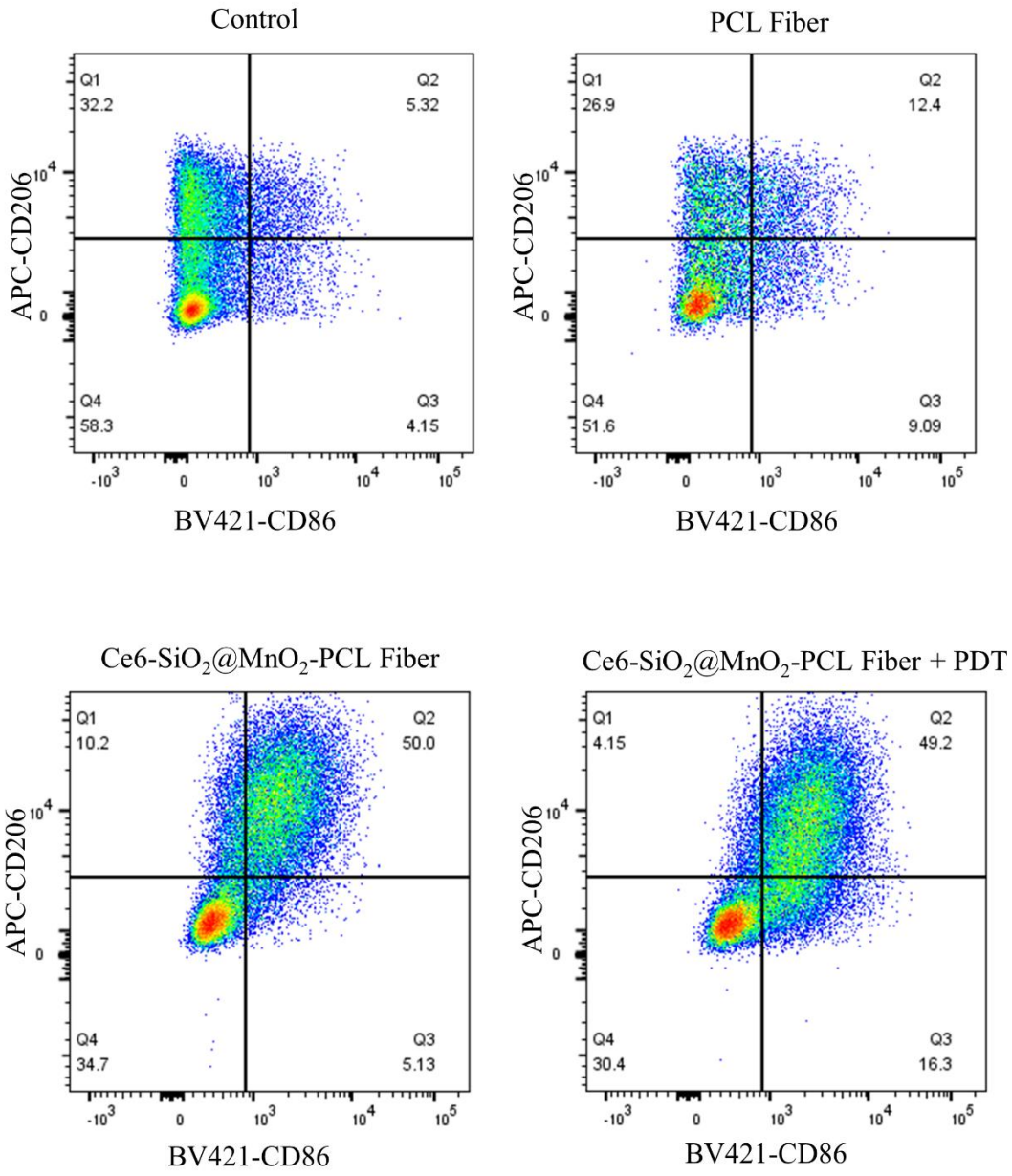

Figure S4. Flow cytometric analysis of tumor associated macrophages (TAMs) in mice under different treatment. CD86 and CD206 are characteristic surface molecules of M1 and M2 type macrophages, respectively.

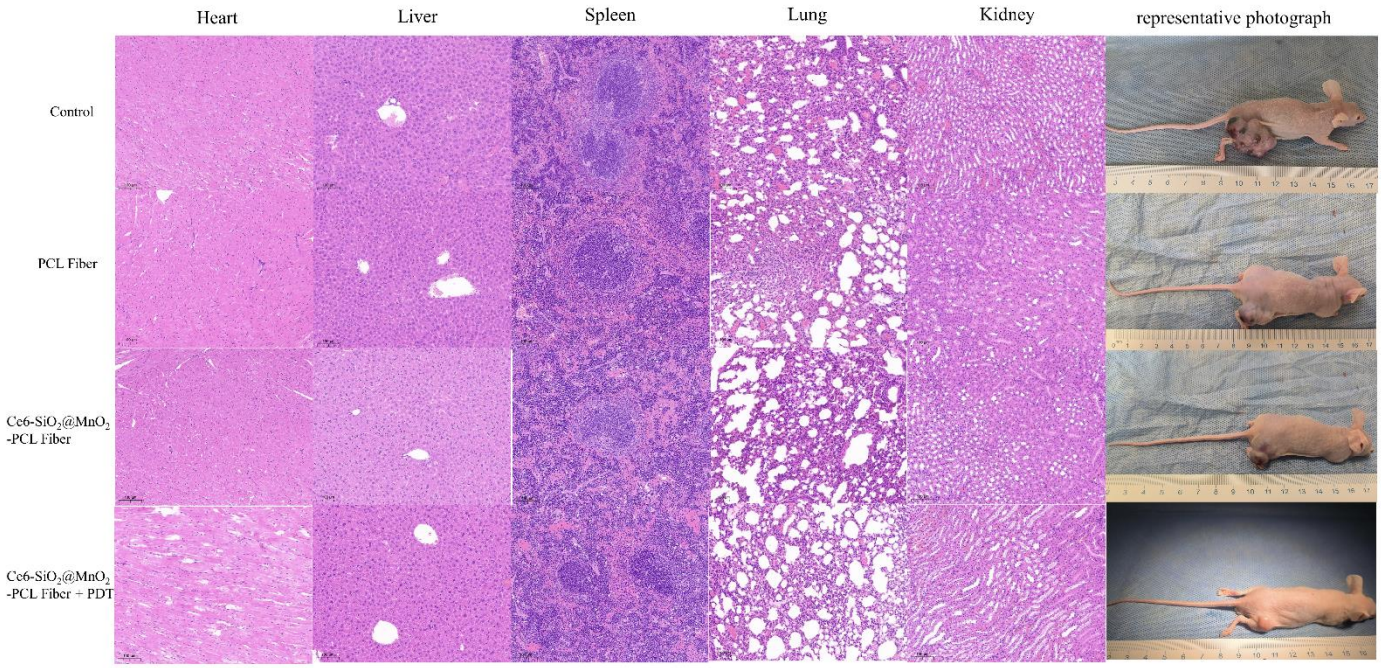

Figure S5. Hematoxylin-eosin (H&E) staining of heart, liver, spleen, lung, kidney and representative photos of AKR mouse subcutaneous tumor models under different treatment.

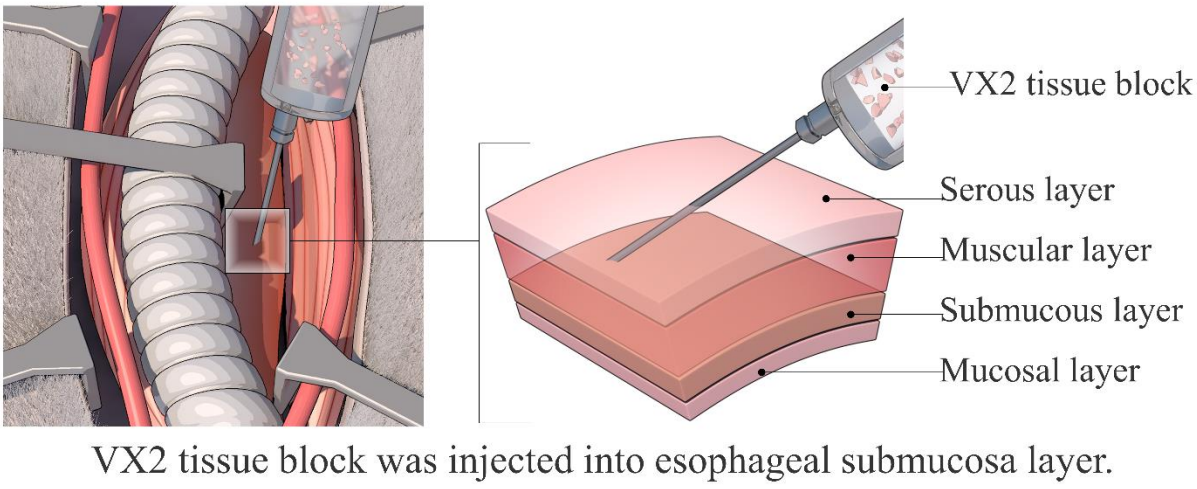

Figure S6. Schematic representation of modeling procedure of malignant esophageal obstruction model in VX2 rabbits.

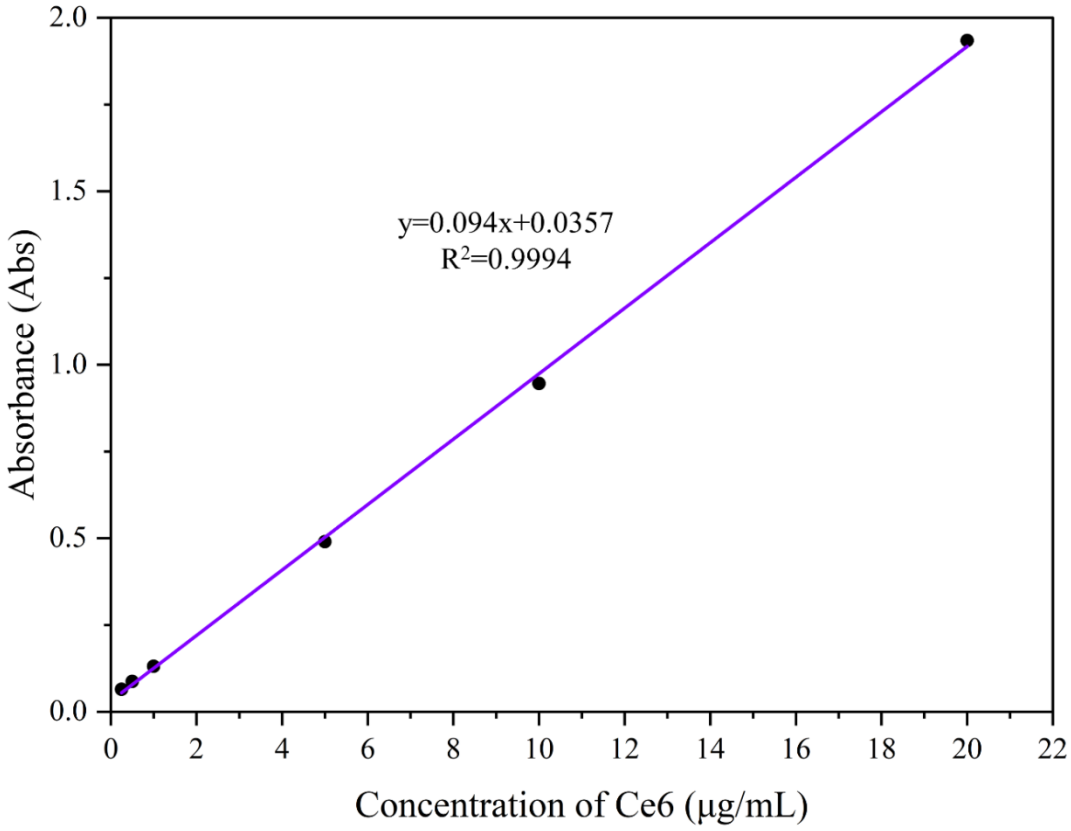

Figure S7. Concentration-absorbance standard curve of Ce6.

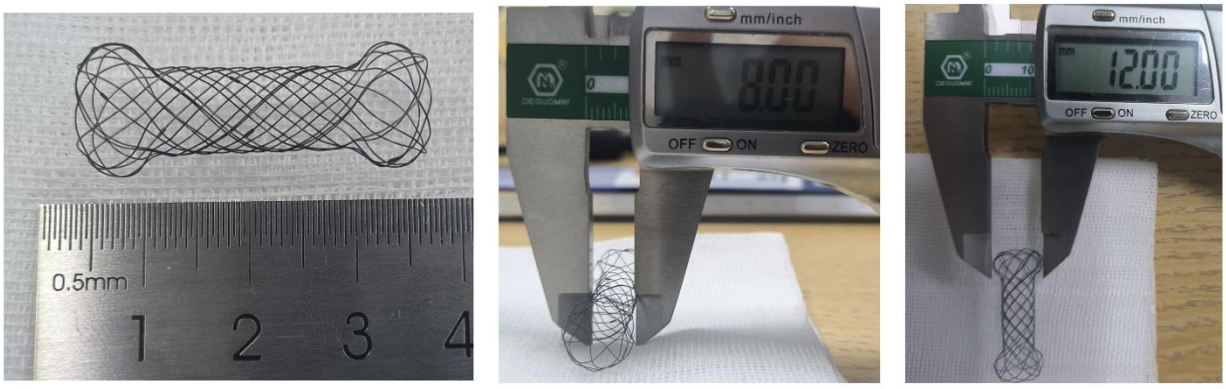

Figure S8. Detailed parameters of the bare esophageal stent.

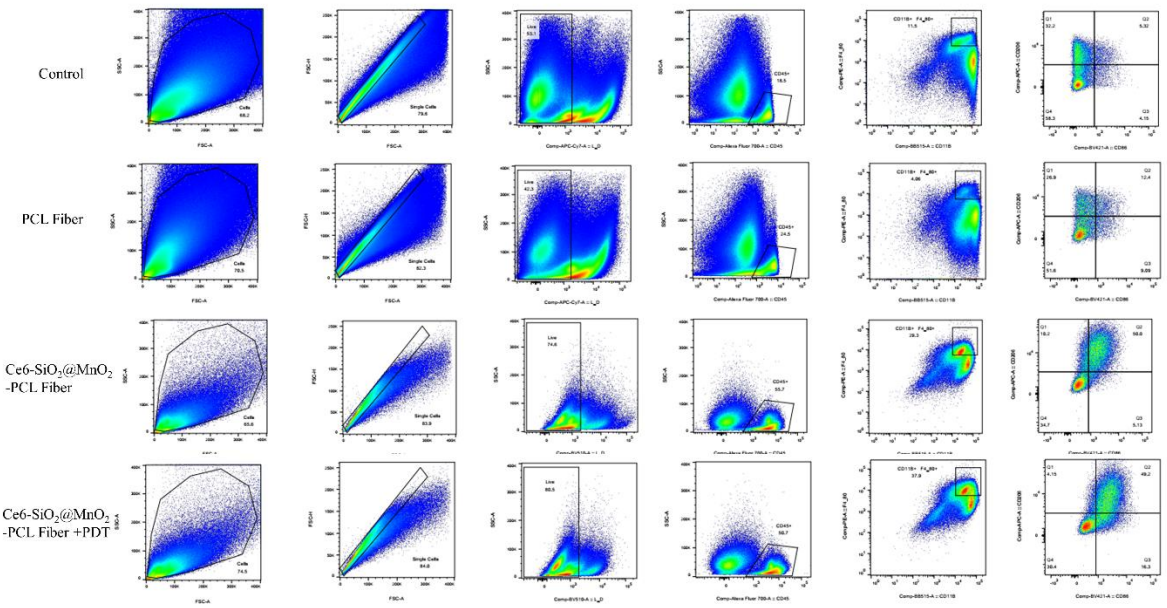

Figure S9. The Loop-gate logic for flow cytometry to detect macrophage polarization. FVS780-CD45+CD11b+F4/80+ cells were defined as living macrophages, among which CD86+ and CD2066+ cells were defined as M1 and M2 macrophages, respectively.

Figure S10. Representative photos of VX2 rabbit malignant esophageal obstruction model treated with intraesophageal photodynamic therapy (PDT).

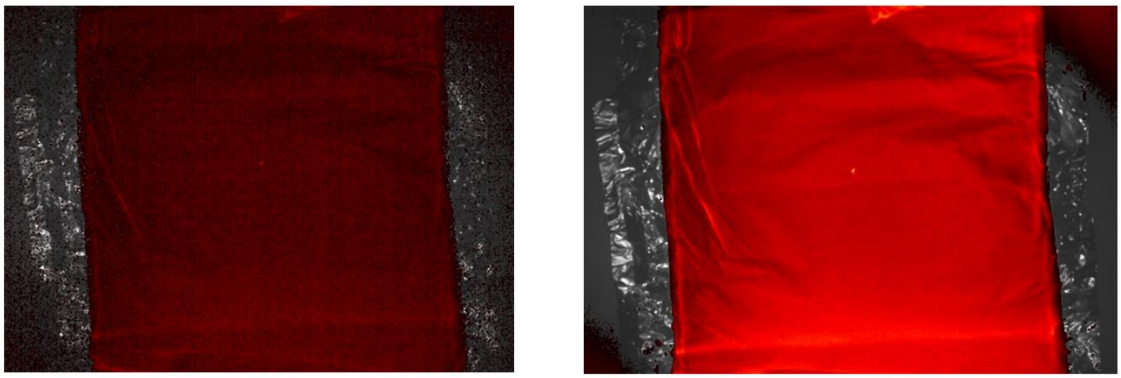

Figure S11. Interactive video information system (IVIS) images of PCL fiber and Ce6-SiO_2@MnO_2-PCL fiber.

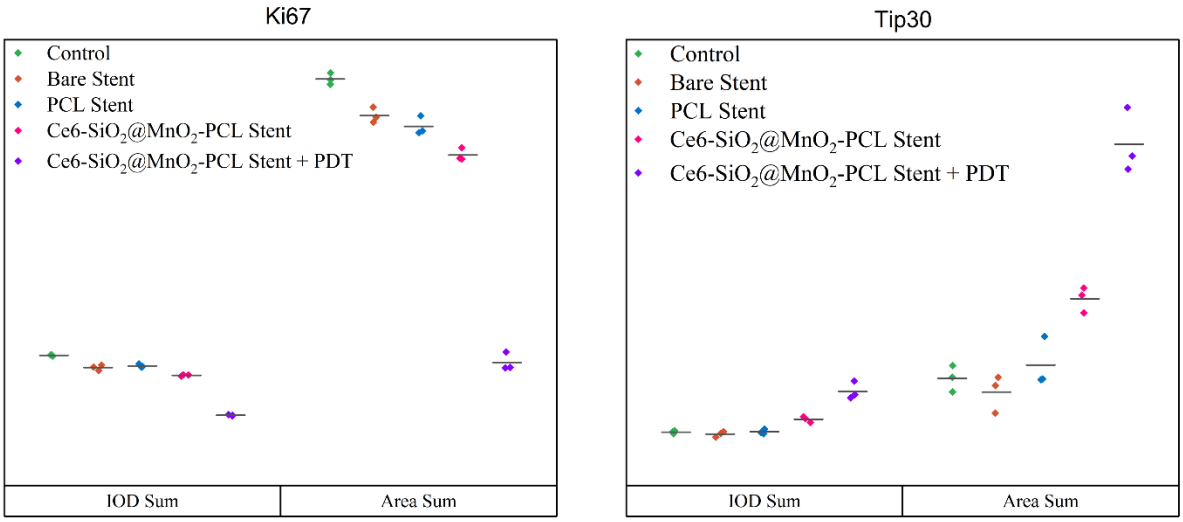

Figure S12. Quantitative analysis of the integrated optical density (IOD) value and the area of the positive region of Ki67/TIP30 in malignant esophageal obstruction model.

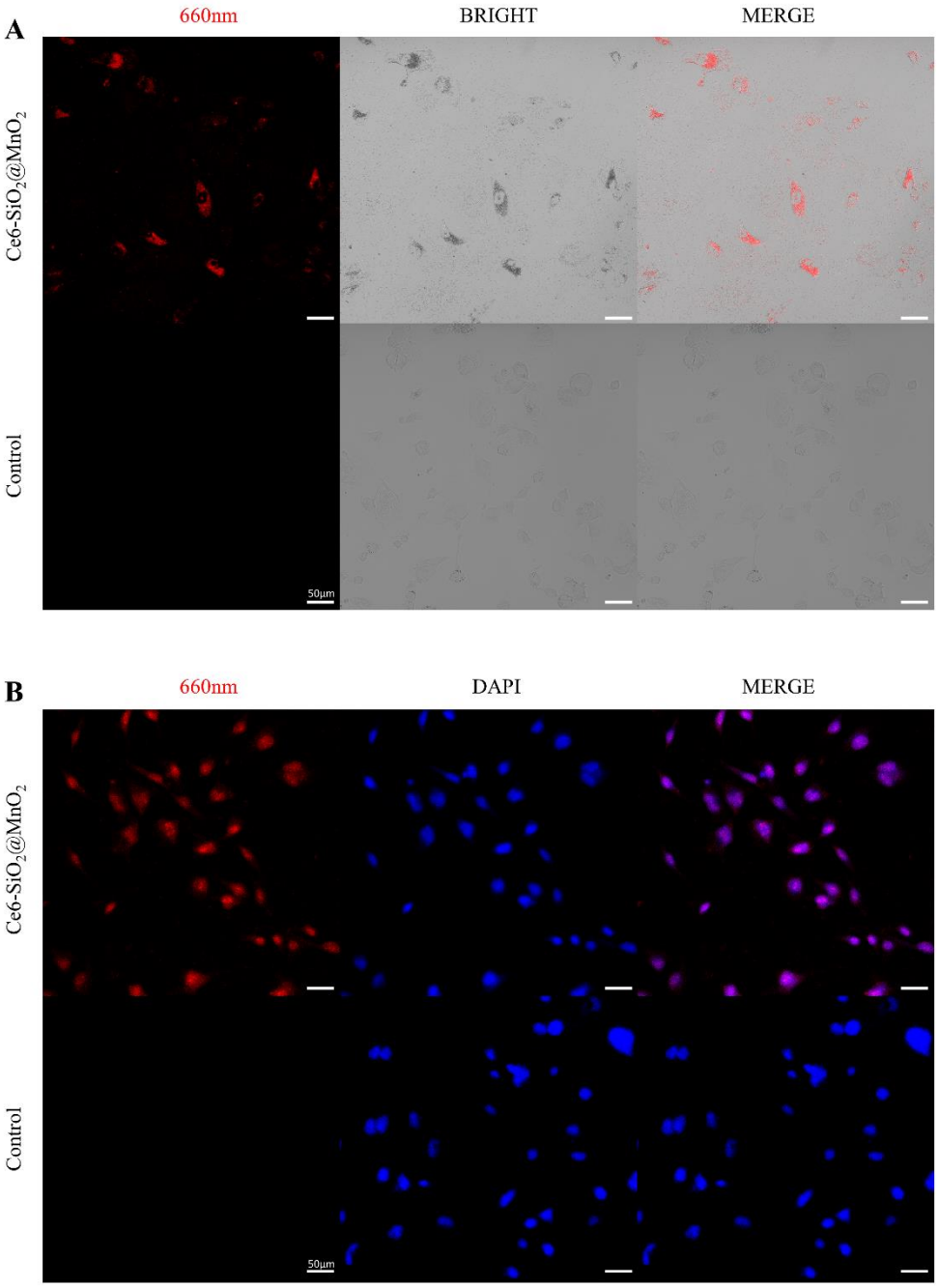

Figure S13. Confocal images of AKR cells incubated with Ce6-SiO_2@MnO_2, PBS for 24 h. A) 660nm channel and bright were applied to observe the distribution of Ce6-SiO_2@MnO_2. B) 660nm channel and DAPI were applied to observe the distribution of Ce6-SiO_2@MnO_2. Red and blue represent Ce6 and DAPI fluorescence, respectively.

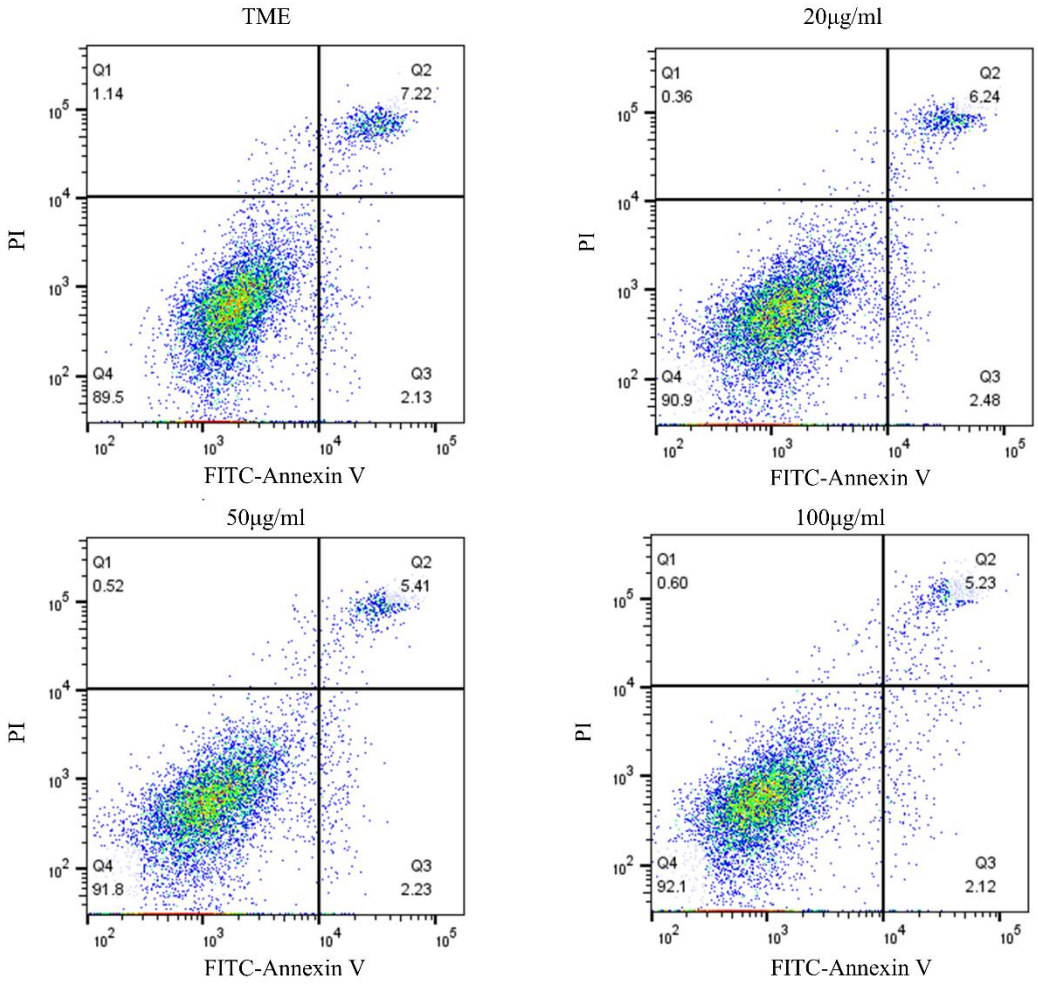

Figure S14. Flow cytometry diagram of apoptosis of AKR cells treated with different concentrations of Ce6-SiO_2@MnO_2 (0, 20, 50, and 100 μg/mL) in TME.

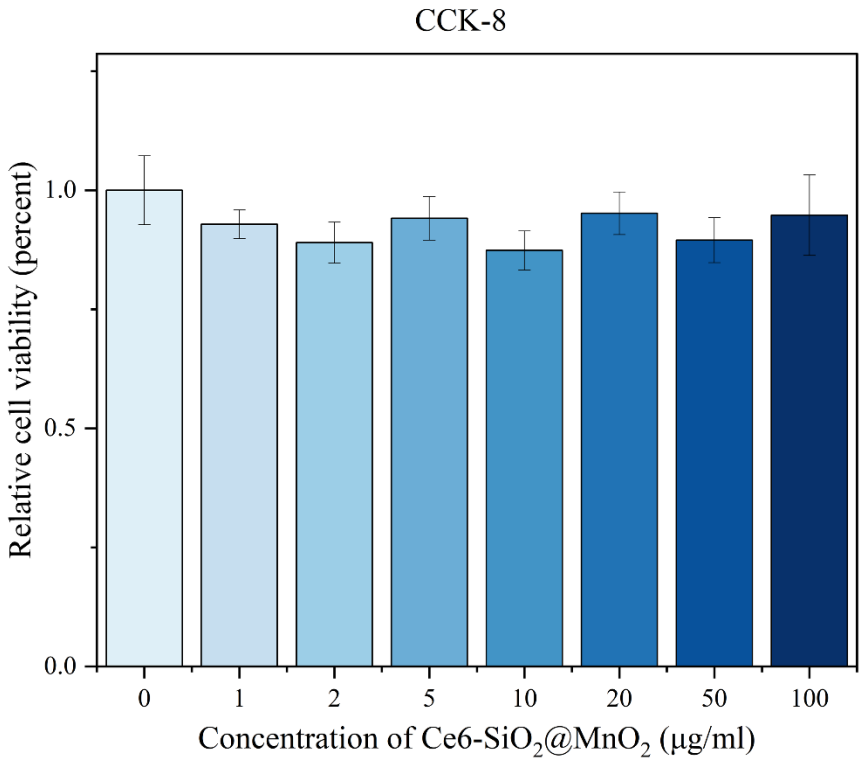

Figure S15. The relative activity of 3T3 cells were detected by CCK-8 experiments with different concentrations of Ce6-SiO_2@MnO_2.

Table S1. Comparison table of PCR primers and sequences.

Primer	Sequence
HMGB1 FORWARD	AGGCTGACAAGGCTCGTTATGAAAG
HMGB1 REVERSE	GGGCGGTACTCAGAACAGAACAAG
STAT1 FORWARD	GCTGCCGAGAACATACCAGAGAATC
STAT1 REVERSE	CCAGTTCGCTTAGGGTCGTCAAG
IL-10 FORWARD	TGGGTTGCCAAGCCTTATCG
IL-10 REVERSE	CTCTTCACCTGCTCCACTGC
TNF-α FORWARD	CGCTCTTCTGTCTACTGAACTTCGG
TNF-α REVERSE	GTGGTTTGTGAGTGTGAGGGTCTG
GAPDH FORWARD	GGCAAATTCAACGGCACAGTCAAG
GAPDH REVERSE	TCGCTCCTGGAAGATGGTGATGG

Table S2. Table of subcutaneous tumor volume over time in AKR mouse.

Tumor volume (mm^3)	0day	2day	4day	6day	8day	10day	12day	14day
Control	126.20	201.82	337.92	556.88	753.40	1130.99	1297.40	1497.10
	114.15	165.77	285.90	537.67	638.00	864.78	949.33	1048.42
	101.48	146.82	248.10	366.53	506.82	652.99	708.60	882.47
PCL	115.38	172.06	291.84	353.01	473.34	683.52	955.85	1140.63
	120.47	156.56	248.35	331.45	457.33	600.14	837.15	1032.79
	102.79	164.93	288.86	383.11	435.90	549.61	651.75	790.79
Ce6-SiO_2@MnO_2 - PCL	121.77	163.93	358.71	360.63	494.55	568.51	664.30	879.33
	108.71	111.88	155.32	155.44	315.80	339.11	413.07	702.27
	116.58	146.56	193.98	258.87	354.61	444.45	614.34	779.54
Ce6-SiO_2@MnO_2 - PCL + PDT	109.44	121.73	99.49	126.51	155.33	203.75	206.35	192.02
	103.45	106.65	128.46	125.41	127.82	139.29	159.90	196.30
	120.73	134.25	174.35	155.89	208.84	242.71	260.90	329.40

Table S3. Magnetic resonance imaging (MRI) sequence parameters

Parameter	T2_tse_dixon_tra	T1_tse_tra	T1_vibe_dixon_tra
Field of view (mm^2)	250 × 250	250 × 250	280 × 238.6
Scan matrix	208 × 320	224 × 320	225 × 352
Voxel size (mm^3)	0.8 × 0.8 × 4.5	0.8 × 0.8 × 4.5	0.8 × 0.8 × 3.0
Echo time (ms)	70	9	2.46
Repetition time (ms)	3800	519	5.65
Slice thickness (mm)	4.5	4.5	3.0
Number of Slice	30	30	60
Flip angle	150	120	10
Acquisition time (min)	1:37	0:49	0:43

Table S4. Energy dispersive X-ray spectroscopy (EDX) elements detection

Parameter	Si	Mn	K
Percentage (%)	76.383	15.950	1.833
3-sigma	2.151	0.373	0.031
Intensity (cps / µA)	0.1062	0.3833	0.1457
Data processing	Quantitative analysis	Quantitative analysis	Quantitative analysis
Test line	Si Ka	Mn Ka	K Ka